Journal of Alloys and Compounds 509 (2011) 775–781

Contents lists available at ScienceDirect

Journal of Alloys and Compounds

journal homepage: www.elsevier.com/locate/jallcom

Influence of extrusion temperature on deformation behavior of C_{sf}/AZ91D composite during semi-solid extrusion

L.Z. Su [a], L.H. Qi [a,*], J.M. Zhou [a], H.J. Li [b]

[a] School of Mechatronic Engineering, Northwestern Polytechnical University, Xi'an 710072, China
[b] School of Materials Science and Engineering, Northwestern Polytechnical University, Xi'an 710072, China

ARTICLE INFO

Article history:
Received 27 May 2010
Received in revised form
10 September 2010
Accepted 18 September 2010
Available online 24 September 2010

Keywords:
Composites
Liquid phase
Deformation behavior
Stream function

ABSTRACT

Deformation behavior and formability of C_{sf}/AZ91D magnesium composite were investigated by semi-solid extrusion between 695 K and 728 K, including temperatures below and above the partial melting temperature. A method of constructing kinematically admissible velocity fields for axisymmetric extrusion based on the theory of flow function was proposed. Flow lines were analyzed in C_{sf}/AZ91D composite after extrusion at elevated temperatures. Based on an analytic flow function, the deformation field was obtained. The results show that when the composite is extruded in a semi-solid state containing a small volume of liquid, the presence of the liquid reduces deformation resistance by relaxing the stress concentrations, and improves the formability of composites as lubricant. However, the gradient of velocity field is increased and deformation uniformity is aggravated at temperatures greater than partial melting point at 701.3 K. A more uniform deformation field was attained at the temperature close to or slightly below the partial melting temperature.

1. Introduction

The extrusion directly following vacuum infiltration (EFVI) as a new forming technique has received much attention in recent years [1,2]. The process can form magnesium matrix composite in the semi-solid state and has a number of advantages, among which near-net-shape characteristics is the most important one. In EFVI, the flow behavior of the materials affects the mechanical properties due to separation phenomena of the solid and liquid phase [3]. Moreover, the fabrication of magnesium matrix composite is more complicated due to high sensitivity of the flow stress to temperature [4–6], which results in undesirable phenomena such as fracture of reinforcement, debonding of interface or map cracking of surface in the extruded product. The knowledge of relationships between deformation mechanisms and temperature in liquid–solid extrusion for composites is very important, in order to form the material under the optimal thermo-mechanic conditions and to improve the mechanical properties in the processed material.

In the earlier work, the extrusion process was simulated with finite element method [7] and upper bound element technique (UBET) [8], but the calculated deformation force was usually larger than that of actual situation due to some assumption and simplified modeling. The simulated results of the deformation behavior in semi-solid zone are not accurate enough. Recently, deformation behavior in semi-solid state has been investigated by compression tests [9–13]. It suggests that mechanisms of deformation are strongly affected by the volume and distribution of a liquid phase. However, it is difficult to investigate deformation uniformity in semi-solid extrusion. The flow line method developed by Arruffat-Massion et al. [14] gives the most realistic solution to the plastic forming problems. The strain field in the deformation zone can be calculated according to the deformation of the flow lines marked on the surface of the specimen. Some experiments have demonstrated that it is more reasonable and easier to analyze the deformation behavior during plastic deformation from the view of metal flow line than the general simple shear theory [15,16].

In this work, semi-solid extrusion for C_{sf}/AZ91D composite was carried out over a temperature range of 695–728 K, including temperatures below and above the partial melting temperature. Then a new and more precise flow field was proposed which used an analytical flow function. The entire flow field can be described by flow-function elements in the form of high-order polynomials. Also, the condition of incompressibility can be satisfied automatically. The velocity, the strain rate and the effective strain were calculated from the flow lines. The effects of extrusion temperature on the deformation uniformity were analyzed.

* Corresponding author. Tel.: +86 29 88460447; fax: +86 29 88491982.
E-mail address: qilehua@nwpu.edu.cn (L.H. Qi).

0925-8388/$ – see front matter.
doi:10.1016/j.jallcom.2010.09.086

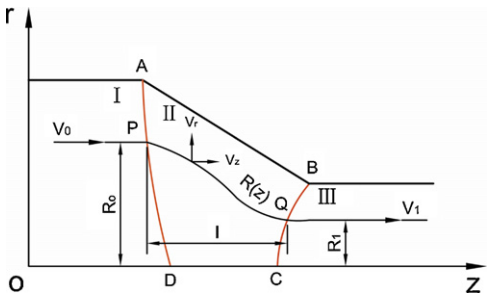

Fig. 1. The illustration of deformation model during extruding composite. The radial and axial coordinates used in this analysis are r and z. The corresponding components of particle velocity are v_z and v_r for a material point moving along the flow line. The circumferential coordinate θ is not shown.

2. Description of the model

2.1. The model of flow line

For the axisymmetric problem of extrusion, we use ordinary cylindrical co-ordinates r, θ, z as indicated by Fig. 1. According to the definition of flow line [17,18], flow line coincides with trace of material particles and is equal to isoclines of the flow function. The infinitesimal dS has the same direction with velocity u on the flow line in three dimensional spaces. Denote the axial- and radial-velocity components of an arbitrary mass particle by v_z and v_r respectively. In addition, it is assumed that the metal flow is steady with no rotation and the velocity component of fluid particle in the circumferential direction is zero (that is $d\theta = 0$, $v_\theta = 0$). The flow field of extrusion process can be considered as the two-dimensional plain flow. Thus, the differential equation of flow-line and continuity equation (for incompressible material) of fluid flow can be expressed as

$$\begin{cases} -v_r dz + v_z dr = 0 \\ \dfrac{\partial v_r}{\partial r} = -\dfrac{\partial v_z}{\partial z} \end{cases} \tag{1}$$

where v_r and v_z are the velocity components of material particle with respect to r and z, respectively.

Eq. (1) can be viewed as a function of total differential equations, it has

$$\begin{cases} -v_r = \dfrac{\partial \varphi}{\partial z} \\ v_z = \dfrac{\partial \varphi}{\partial r} \end{cases} \tag{2}$$

Then, the differential equation of flow line can be written as

$$d\varphi(r, z) = 0 \tag{3}$$

That is

$$\varphi(r, z) = C \tag{4}$$

where C is an arbitrary constant. The flow function $\varphi(r, z)$ can best be understood as the volume rate of axial flow through a circle of radius r, concentric with the axis at z. For isochoric deformation the density is constant and so φ is proportional to the mass rate of flow. The material flow can be described in term of the size of a given amount of material passes through at various stations on its way downstream. The envelope of all circles passing material at the same mass flow rate is a surface of a constant φ and the intersection of a plane containing the axis of symmetry with this envelope is a flow line.

During relatively steady flow of the billet through the die, it seems unlikely that adjacent particles in the same cross-section has oppositely directed radial-velocity components if the flow is axisymmetric. Therefore, material particles flow along lines of constant φ and the velocity field is specified by Eq. (2).

2.2. The equation of flow line for extruding composite

Fig. 1 shows the deformation process of extruding composite. Point O is the centre of billet. In the deformation model, the forming zone is divided into three regions. Region I and Region III are the rigid zone, in which the material moves rigidly downward with a constant ram speed of v_0. Region II is separated from Region I by the entry surface and Region III by the exit surface. The intersection lines AD and BC are called the velocity discontinuity line. Far upstream from the die, material will have the same velocity as the ram. Far downstream from the die material will have the velocity v_1 of the extruded product. We denoted that R_0 is the initial (upstream) radius, R_1 is the outer (downstream) radius of a given flow line, l is the length of plastic deformation zone, and R is the radial radius of cross-section outline in the deformation zone. The other signs are shown in Fig. 1.

If the equation of flow line during extrusion process is given as $R = R(z)$, it can be expressed by a third-order even polynomial:

$$R(z) = a_1 z^3 + a_2 z^2 + a_3 z + a_4 \quad 0 \le z \le l \tag{5}$$

Based on the assumption of plane strain flow in the extruding process, it can be shown that the sizes of the entrance and outer of die are the overall dimensions of billet and product, respectively. The metals have no radial flow at the beginning and ending of extrusion, namely $v_r = 0$. That is, in Eq. (2), the tangent vector along the z-direction is equal to zero at the entrance and outer zone of flow line, $\partial\varphi/\partial z = 0$. Thus, the boundary conditions of flow line equation are

$$\begin{cases} R(z) = R_0 \dfrac{\partial R}{\partial z} = 0 \quad z = 0 \\ R(z) = R_1 \dfrac{\partial R}{\partial z} = 0 \quad z = l \end{cases} \tag{6}$$

Substituting Eq. (6) into Eq. (5), it can be written as

$$\begin{cases} a_1 = \dfrac{2(R_0 - R_1)}{l^3} \\ a_2 = \dfrac{-3(R_0 - R_1)}{l^2} \\ a_3 = 0 \\ a_4 = R_0 \end{cases} \tag{7}$$

Denoting $f(z) = 3(z/l)^2 - 2(z/l)^3$, the equation of flow line can be concluded:

$$R(z) = R_0[1 - f(z)] + R_1 f(z) \tag{8}$$

2.3. The kinematically admissible velocity fields

The velocity fields coinciding with the above conditions are called kinematically admissible velocity fields [19]. Accordingly, the axis velocity v_0 and v_1 satisfy the incompressibility conditions given by $v_1 = v_0(R_0/R_1)^2$ at the rigid zone. To express the shape of flow line for particles in deformation zone, the parameter ξ which is the function of r and z is introduced as

$$\xi = \xi(r, z) = \text{constant}$$

So, a equation of flow line can be determined as corresponding to a value of ξ. According to the model as shown in Fig. 1, the flow line is expressed by third-order polynomial. The parameter ξ of each flow line must meet the flowing conditions:

$$\begin{cases} \xi = 0 \quad \text{when} \quad r = 0 \\ \xi = R_0^2 \quad \text{when} \quad r = R(z) \end{cases} \tag{9}$$

Defining $\lambda = (R_0 - R_1)/R_0$, so

$$\xi = {R_0}^2 \frac{r}{R(z)} = \frac{R_0 r}{1 - \lambda f(z)} \tag{10}$$

According to Eq. (10), the flow function is $\varphi = f(\xi)$. The velocity field can be concluded:

$$\begin{cases} v_\theta = 0 \\ v_r = -\dfrac{\partial \varphi}{\partial z} = -\dfrac{\partial \xi}{\partial z} f'(\xi) \\ v_z = \dfrac{\partial \varphi}{\partial r} = \dfrac{\partial \xi}{\partial r} f'(\xi) \end{cases} \tag{11}$$

Because the flow function $f(\xi)$ satisfies the velocity boundary condition as the case of $v_z = (R_0/[1 - \lambda f(0)])f'(\xi) = v_0$, when $z = 0$, it results

$$f(\xi) = v_0 \frac{\xi}{R_0} = \frac{v_0 r}{1 - \lambda f(z)} \tag{12}$$

By Eq. (12), the final component of velocity field can be derived

$$\begin{cases} v_\theta = 0 \\ v_r = -\lambda r f'(z) v_0 \dfrac{1}{[1 - \lambda f(z)]^2} \\ v_z = v_0 \dfrac{1}{1 - \lambda f(z)} \end{cases} \tag{13}$$

Since the flow function has been established accurately, the strain-rate components can be determined at each point (r, z) by further differential coefficient and the following definitions:

$$\begin{cases} \dot{\varepsilon}_r = -\dot{\varepsilon}_z = -\dfrac{\partial v_z}{\partial z} \\ \dot{\varepsilon}_{rz} = \dot{\varepsilon}_{zr} = \dfrac{1}{2}\left(\dfrac{\partial v_z}{\partial r} + \dfrac{\partial v_r}{\partial z}\right) \end{cases} \tag{14}$$

It should be noted that these definitions relate the instantaneous strain rates to the current co-ordinates of each material point rather than the original co-ordinates of the point. Hence, they are the rates of logarithmic or "true" strain components. For the plane strain, there are only four strain components while others are equal to zero.

Another variable $\dot{\bar{\varepsilon}}$, the square root of the quadratic invariant of the strain-rate deviator tensor, or 'effective strain rate', can be defined as

$$\dot{\bar{\varepsilon}} = \frac{\sqrt{2}}{3}\sqrt{(\dot{\varepsilon}_\theta - \dot{\varepsilon}_r)^2 + (\dot{\varepsilon}_r - \dot{\varepsilon}_z)^2 + (\dot{\varepsilon}_z - \dot{\varepsilon}_\theta)^2 + 6\dot{\varepsilon}_{rz}^2} \tag{15}$$

3. Materials and methods

Short carbon fibers (C_{sf}), made in Jilin Carbon Co., Ltd., China, with a length of 3–5 mm and in diameter of 7 μm, were selected to fabricate the carbon fiber preform. AZ91D alloy was used as the matrix material of magnesium matrix composites. The chemical composition of AZ91D alloy is shown in Table 1. The liquidus and the solidus temperature of the alloy are 868 K and 743 K, respectively. The 10 vol.% short carbon fiber-reinforced AZ91D magnesium matrix composite billets were prepared by a gas pressure infiltration process [20].

The experiments were carried out by extruding the C_{sf}/AZ91D composite in the condition of an extrusion ratio 4:1 and 35° of the die angle. The initial dimension of the specimen was Ø45 mm × 30 mm. A grid of spacing 3 mm × 3 mm and line depth of 1.5 mm representing the flow lines and transverse lines was engraved on the internal surface using a linear cutting machine. Then, the bifid billet was put into the container to be extruded out with a forward punch velocity of 5 mm/s.

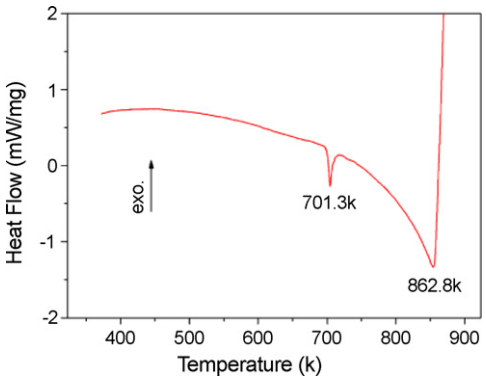

Fig. 2. The result of the DSC experiment for C_{sf}/AZ91D composite sample, showing that the partial melting temperature is 701.3 K.

Table 2
The liquid phase fraction at the conditions of different extrusion temperature.

Material	Extrusion temperature (K)	Liquid-phase fraction (%)
C_{sf}/AZ91D composite	728	4.8
	709	0.446
	695	0

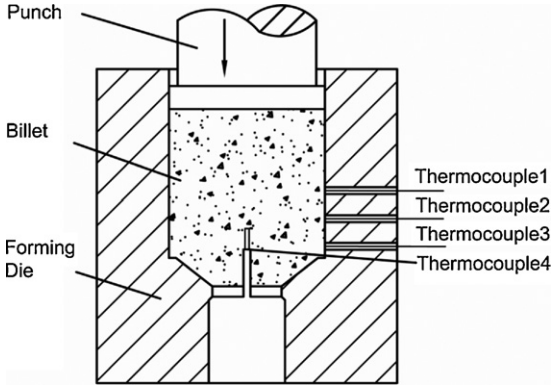

Fig. 3. The distributions of measuring thermocouples in material and forming die. The distance of the thermocouples from the bottom of the forming die are 140 mm, 100 mm and 60 mm, respectively and Thermocouple4 is 15 mm from the bottom of the initial billet in the core.

A differential scanning calorimetry (DSC) experiment was carried out on a type of NETZSCH-STA 449C with heating rate of 15 K/min under the protection of nitrogen atmosphere. The DSC run started at room temperature and ended at about 923 K. The thermal analyzer was connected to a computer with a suitable interface, and the data from the run were continuously stored. Fig. 2 shows the DSC trace of C_{sf}/AZ91D composite obtained by heating the composite from 373 K to 923 K. The DSC trace has two endothermic peaks at the temperature 701.3 K and 862.8 K, respectively. The small endothermic peak is attributed to partial melting at the matrix/reinforcement interfaces and at grain boundaries [10,21]. According to the DSC trace, the composites were extruded at various temperatures above or below partial melting point.

To study the effects of temperature on the deformation behavior of C_{sf}/AZ91D composites, the extrusion temperatures were identified as 728 K, 709 K and 695 K. The liquid fractions at different temperature were shown in Table 2. In order to analyze the effects of parameters on the forming process, extrusion pressure, displacement and temperature were monitored through the data acquisition system [22]. The temperature of the composite billet in the container was monitored through the K-type thermocouples. In which, a thermocouple was embedded in

Table 1
The chemical composition of AZ91D alloy (w%).

Content of alloying elements (%)					Density (g/cm³)	Solidus (°C)	Liquidus (°C)
Al	Zn	Mn	Si	Mg			
9.1	0.84	0.30	0.04	Rest	1.81	470	595

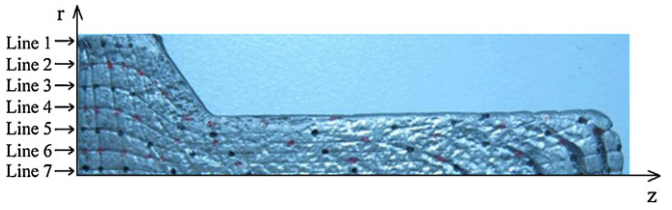

Fig. 4. The deformed grid photograph of C_{sf}/AZ91D composite fabricated by extrusion at 728 K. The deformation body keeps axisymmetric during extrusion process and a half of the deformed grid is considered.

the billet and other three thermocouples were distributed on the die wall. The locations are shown in Fig. 3. After the required temperature was reached, the ram was moved for extrusion and the moving velocity of the ram is changed according to the applied extrusion pressure.

After extruding at 695 K, the samples were extracted from the die, and the deformed grid or the flow pattern was photographed as shown in Fig. 4. Based on Eq. (5), the third-order polynomial approximations was constructed to fit flow line, i.e. each flow line was expressed by $r_j = \sum_{n=0}^{3} a_{jn} z^n$ and the coefficients a_{jn} were determined by least-squares fitting of the measured point (z, r) corresponding to flow line j, respectively. These polynomials were then used to obtain interpolated 'data' points by subdividing the intervals Δz between axial stations and evaluating all of the $r_j(z)$ points for the original and intermediate stations by using the polynomials. The smoothing of the flow line for the billet is shown in Fig. 5.

4. Results and discussion

The velocity of each point in r- and z-direction can be calculated by Eq. (13). The strain rates and von Misses equivalent strain rate can be obtained from Eqs. (14) and (15). Fig. 6 shows the velocity components along the flow line as a function of r axis position at various axial stations at different extrusion temperature, respectively. The results show clearly that the material flow mainly

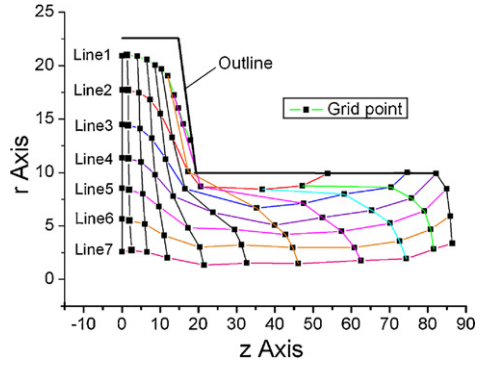

Fig. 5. The smoothing of the flow line computed from flow-function analysis based on the experimental result in Fig. 4.

concentrates on the deformation band near the outlet of the forming die. In zone I and zone III, the material flows almost vertically in the container and the forming die. When material enters the zone II, the flow direction changes dramatically at the transition corner between container and forming die and large plastic deformation was taken on. The velocity gradients of transverse and longitudinal direction are large. Due to the effects of friction and temperature, the flow velocity of material near to the outline of die is less than that along the centre line. Furthermore, the 'dead zone' exists at the round radius of die along the flow line 1. Compared from (a) to (c) in Fig. 6, it can be seen that with the velocity gradient along r-axis direction and the 'dead zone' become large with the extrusion temperature increasing. As the extrusion temperature is 695 K, the deformation has the best symmetry and trends to flow evenly.

Fig. 7 shows the vertical velocity distributions of different points on the flow lines at the entrance located from point a′ to point a

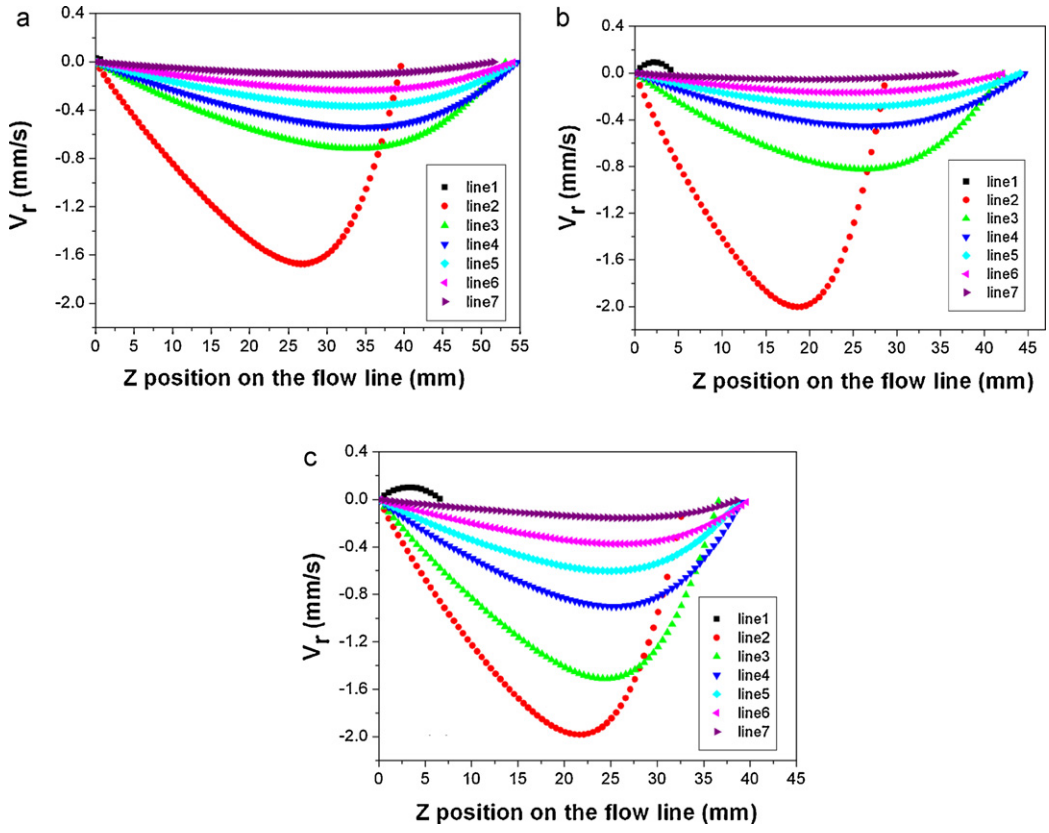

Fig. 6. Normal velocity components u along the flow line as a function of radial position at various axial stations. The extrusion temperature is: (a) T = 728 K; (b) T = 709 K; (c) T = 695 K.

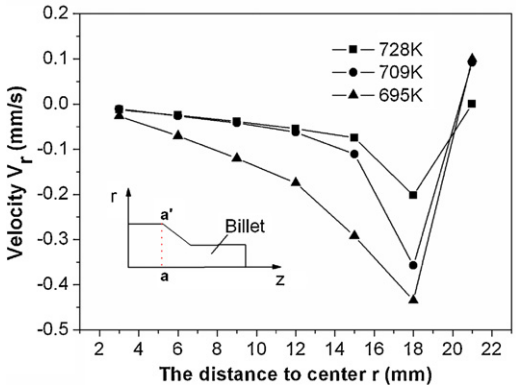

Fig. 7. The effects of extrusion temperature on the vertical velocity distributions of different points on the flow lines at the entrance of the zone II.

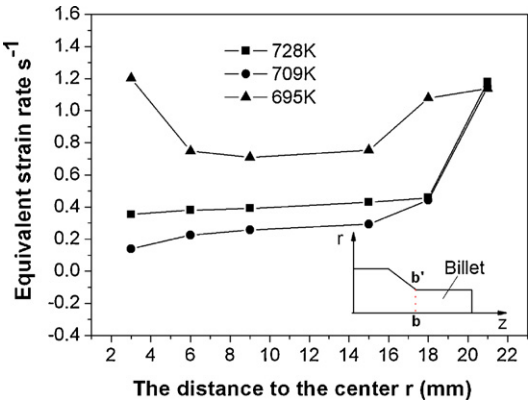

Fig. 9. The effects of extrusion temperature on the equivalent strain rate distributions of different points on the flow lines at the outlet of the II region.

of the zone II at three extrusion temperature. It is clear that the vertical velocity close to the die wall rises with the temperature increasing. This effect is more obviously along flow line number 2. When the extrusion temperature is 695 K, the velocity variation between line 1 and line 2 is largest. To analyze this phenomenon comprehensively, it is a significant increase in the friction force that is responsible for the present observations. When the extrusion temperature is elevated, the sample is swelling. It produces high pressure on the die walls and high friction force which leads to develop the 'dead zone' in the outlet corner of the die.

Fig. 8 shows von Misses equivalent strain rate along the flow line as a function of radial position at various axial stations. It can be seen that the strain rate varies strongly along the flow line. The von Misses equivalent strain rate is zero at the entrance section and increases forward the exit section along the boundary. Otherwise, the equivalent plastic strain of the material in the extruder is relative low and there is no large plastic deformation in the extruder. The plastic strain rate in the extruded billet is lower than that at the outlet of the forming die. This is because the material at the outlet of the forming die undergoes large plastic deformation, while the extruded billet undergoes no further deformation.

In order to obtain proper information about the uniformity of the material, variation of the equivalent strain rate across outlet of the die located from point b′ to point b was analyzed as shown in Fig. 9. It is indicated that the deformation in the core enhances with the extrusion temperature increasing when the temperature is over the solidus. The reason is that the forming process is accomplished under semi-solid state. So the material stays in different

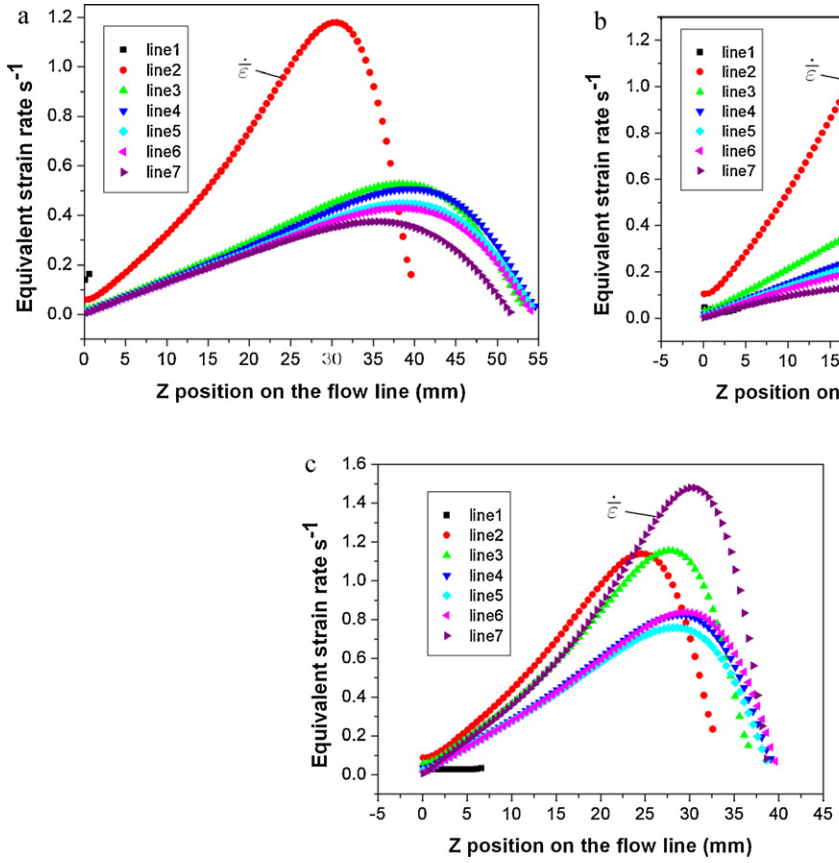

Fig. 8. The von Mises equivalent strain rate along the flow line as a function of radial position at various axial stations: (a) $T = 728$ K; (b) $T = 709$ K; (c) $T = 695$ K.

state at the surface and inner part during the extrusion. The material flows easier as the temperature is higher. Making the material easy-to-filling through the corner of die, and fuller shear deformation can be obtained. However, the deformation uniformity is not improved. While the extrusion temperature is under the solidus, it can greatly increase the strain level accumulation without reducing the uniformity of the strain distribution.

This phenomenon is a result of different flow behaviors of the solid globules with liquid phase. No liquid existed as the C_{sf}/AZ91D composite was extruded at 695 K and the dominant deformation process was plastic deformation based on solid-phase in the interior of grains. Partial melting started at 709 K and the primarily melted liquid phase was discontinuously dispersed at grain boundaries. At this time, the role of liquid as a lubricated flow was not obvious. The dominant deformation mechanism was still plastic deformation of the solid phase within the grain, with a small amount of grain boundary sliding. When the extruding temperature reached 728 K, the volume fraction of liquid was 4.8% and continuously dispersed. There were more grain-boundaries and interfaces participating in the relative sliding, and solid-phase particles existed in the form of skeleton due to the presence of liquid phase. The dominant deformation mechanism was changed to grain boundary sliding with a small amount of plastic deformation in the crystal [10].

The deformation mechanism by extrusion for the C_{sf}/AZ91D composite containing a small volume of liquid is suggested as follows. In semi-solid extrusion process, the hydrostatic pressure acting on the liquid-phase close to lateral die wall is most under the role of friction and decreases along the radius direction. During the initial stage of deformation, the liquid outside flows to smaller hydrostatic pressure region through the grain boundary drove by large hydrostatic pressure. At the same time, due to the center is a large deformation zone, the internal liquid transfers to lateral die wall through the grain boundary, thus makes the thickness of the liquid phase increase on the grain boundary. Such a thick liquid phase improves the role of lubrication flow at liquid boundaries and causes a large decrease in stress, resulting in grain boundary sliding occurs prior to the occurrence of flow localization. Therefore, it is suggested that the maximum equivalent strain rate on the flow line 2 in the specimen containing a small amount of liquid is obtained because the local deformation rate at the liquid boundaries is accelerated due to the presence of a small amount of liquid as shown in Fig. 8(a) and (b). The result for the deformation mechanism of material containing a small volume of liquid is in agreement with pervious studies [10,23]. When extrusion is performed below the solidus temperature, the dominant deformation mechanism is dislocation creep controlled by lattice diffusion of the matrix [24]. On the plastic deformation stage, the stress value increases, corresponding increase of the required load. Furthermore, the heat generated by plastic work is important for the temperature field distribution in the extrusion process. The partial melting in the sample core occurs with the temperature is above the partial melting temperature as shown in Fig. 10. This can cause the material at the core part has better flow. Thus it can be indicated that the equivalent strain rates on the die wall and core are larger than that in the middle part of specimen as the extrusion temperature is 695 K in Fig. 8(c).

Fig. 11 shows the extrusion pressure and extrusion velocity with the extrusion temperature in a normal condition according to experimental measuring results. The initial ram velocity was 5 mm/s. It can be found that increasing the extrusion temperature decreased the extrusion pressure and increased the extrusion velocity. This is caused by the decreased flow stress of materials at high temperatures. When the extrusion temperature varies from 695 K to 728 K, the deformation force reduces rapidly to a smaller

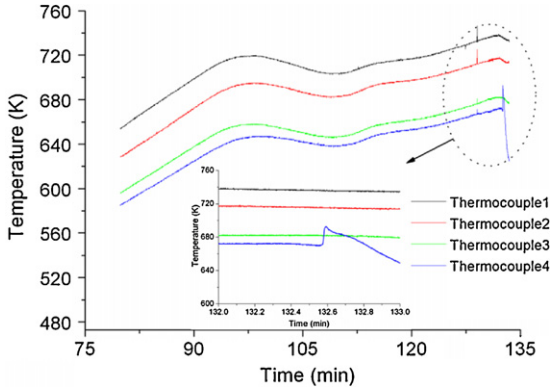

Fig. 10. Temperature variation of billet at different parts during thixo-extrusion process.

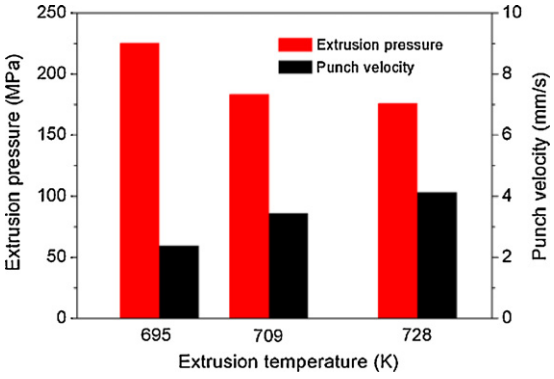

Fig. 11. Variations of the extrusion pressure and extrusion velocity with the extrusion temperature on the initial punch velocity of 5 mm/s.

value because the ratio of liquid phase increases. The low load can improve die life and reduce maintenance requirements. However, to consider the deformation uniformity based on the analysis above, the higher surface quality and performance can be obtained at near solidus temperature.

5. Conclusions

A new analytical flow line field has been carried out in order to investigate the plastic deformation behavior of the C_{sf}/AZ91D composite material during the hot extrusion process. From the results obtained, the following conclusions can be drawn:

1. The proposed flow line model using stream function can automatically satisfy the incompressibility and velocity boundary conditions within the die. It gives a varying deformation field along the flow line in good analysis at different extrusion temperatures.
2. The formability strongly depends on the temperature. In particular, excellent formability was attained at temperatures greater than partial melting point of 701.3 K. However, the velocity gradient and deformation uniformity are aggravated due to the present of liquid.
3. A larger deformation zone and the higher deformation uniformity develop under the extrusion temperature adjacent to solidus temperature.
4. It was pointed out that the deformation in this temperature range from 695 K to 728 K is likely to be the lubricated flow in a semi-solid state containing a continuous liquid. In this region, ductility is low as a reflection that extrusion force decreases with the extrusion temperature increasing.

Acknowledgment

The authors thank to the National Nature Science Foundation of China (50972121) and Science and Technology Innovation Foundation of Northwestern Polytechnical University (2010KJ0202) for financial supports.

References

[1] L.X. Hu, S.J. Luo, W.C. Huo, J. Mater. Process. Technol. 49 (1995) 287–294.
[2] L.H. Qi, H.J. Li, P.L. Cui, Trans. Nonferrous Met. Soc. China 13 (4) (2003) 803–808.
[3] L.H. Qi, J.M. Zhou, L.Z. Su, Solid State Phenom. 141–143 (2008) 91–96.
[4] T.J. Chen, X.D. Jiang, Y. Ma, Y.D. Li, Y. Hao, J. Alloys Compd. 497 (2010) 147–154.
[5] Y.W. Wu, K. Wu, K.K. Deng, K.B. Nie, X.J. Wang, X.S. Hu, M.Y. Zheng, J. Alloys Compd. (2010), doi:10.1016/j.jallcom.2010.07.043.
[6] B.H.L.M. Peng, B.R. Powell, M.P. Balough, R.C. Kubic, A.K. Sachdev, J. Alloys Compd. 504 (2010) 527–534.
[7] L.H. Qi, L.Z. Su, C.X. Jiang, J.M. Zhou, Mater. Sci. Eng. A 454–455 (2007) 608–613.
[8] X.Q. Ren, L.X. Hu, X.M. Sun, Acta Metall. Sin. 32 (1996) 551–556.
[9] A. Khosravani, H. Aashuri, P. Davami, A. Narimannezhad, R. Hadian, J. Alloys Compd. 477 (2009) 822–827.
[10] Y. Chino, M. Kobata, H. Iwasaki, M. Mabuchi, Acta Mater. 46 (2003) 3309–3318.
[11] Z.D. Zhao, Q. Chen, Z.J. Tang, C.K. Hu, J. Alloys Compd. 497 (2010) 402–411.
[12] Z.J. Li, W.D. Fei, H.Y. Yue, L.D. Wang., Compos. Sci. Technol. 67 (2007) 963–973.
[13] S. Benke, S. Dziallach, G. Laschet, U. Prahl, W. Bleck, Computat. Mater. Sci. 45 (2009) 633–637.
[14] R. Arruffat-Massion, L.S. Tóth, J.P. Mathieu, Scripta Mater. 54 (2006) 1667–1672.
[15] S.M. Fatemi-Varzaneh, A. Zarei-Hanzaki, M. Naderi, AliA. Roostaei, J. Alloys Compd. 477 (2010), doi:10.1016/j.jallcom.2010.07.157.
[16] A Hasani, L.S. Tóth, Scripta Mater. 61 (2009) 24–27.
[17] L.L. Jia, J.Z. Gao, Chin. J. Mech. Eng. 38 (2002) 92–95.
[18] A. Hasani, R. Lapovok, L.S. Tóth, A. Molinari, Scripta Mater. 58 (2008) 771–774.
[19] Y.T. Lin, J.P. Wang, J. Mater. Process. Technol. 35 (1992) 151–163.
[20] H.B. Ouyang, H.J. Li, L.H. Qi, Z.J. Li, J. Mater. Sci. 43 (2008) 4618–4624.
[21] G.H. Fan, L. Geng, Z.Z. Zheng, G.S. Wang, Y.C. Feng, Mater. Sci. Eng. A 496 (2008) 281–284.
[22] J.M. Zhou, L.H. Qi, J.T. Guan., Solid State Phenom. 141–143 (2008) 85–89.
[23] H. Iwasaki, T. Mori, M. Mabuchi, K. Higashi, Acta Mater. 46 (1998) 6351–6360.
[24] Y.N. Chena, J.F. Wei, Y.Q. Zhao, Mater. Sci. Eng. A 520 (2009) 16–22.